Experimental and theoretical investigation of railway wheel squeal

S S Hsu[1], **Z Huang**[2], **S D Iwnicki**[1*], **D J Thompson**[2], **C J C Jones**[2], **G Xie**[1], and **P D Allen**[1]
[1]Rail Technology Unit, Manchester Metropolitan University, Manchester, UK
[2]Institute of Sound and Vibration Research, University of Southampton, Southampton, UK

The manuscript was received on 2 May 2006 and was accepted after revision for publication on 20 September 2006.

DOI: 10.1243/0954409JRRT85

Abstract: The tangential contact forces that arise at the interface between the wheel of a railway vehicle and the rail provide all the traction, braking, and guidance required by the vehicle. These forces are the result of microslip or creepage and can become unstable exciting vibration of the wheel, particularly at frequencies corresponding to the wheel's axial (and radial) modes.

Although theories exist for predicting these creep forces and their relationship to creepages, most lack experimental verification in the characterization of the falling friction coefficient during unsteady squealing. This paper presents some new results from a project which aims to develop a complete, validated model of curve squeal noise generation accounting for friction characteristics, excitation due to unstable forces between the wheel and rail and vehicle dynamic behaviour. The model includes wheel and track dynamic response and acoustic radiation. As part of the project, a twin disc rig has been modified to provide experimental data for the validation of the model and measurements were made of the lateral force and dynamic response of the rollers due to varying amounts of lateral creepage during squealing. The main feature of the twin disc rig compared with previous research [**1**] is that the contact force measuring system measures the contact forces at the web of the rollers and therefore close to the contact patch and through a slip-ring arrangement enables the lateral vibration of both rollers in relation to squeal be measured with relative ease.

In this paper, detailed descriptions of the twin disc rig and the test method developed are given. An outline of the squeal model is also presented. Results from the tests have been compared with the prediction from the squeal model and with available theories and showed good agreement.

Keywords: twin disc rig, contact forces, squeal noise prediction

1 INTRODUCTION

Curve squeal has been found to originate from the unstable response of a railway wheel when subject to large creep forces while negotiating curved track. Pure tone components of squeal in the range of 600 –10 000 Hz are generally related to wheel natural frequencies that correspond to the out-of-plane wheel bending (or axial) modes.

It is generally thought that the excitation of the squealing wheel originates from a 'stick-slip' mechanism in the contact region. The three main situations considered are lateral creepage at the contact between the wheel tread and the crown of the rail; wheel flange sliding on the gauge face of the rail, and longitudinal creepage at the wheel treads due to differential slip. In a review of curve squeal models by Remington [**2**], squeal due to lateral creepage of the wheel tyre was identified as the most significant cause and the majority of models account specifically for this. The development of treatments has aimed to limit the disturbance of the wheel in this way, as well as the wheel's response to it. Experimental findings and observations have sometimes shown conflicting trends particularly in regard to the

Corresponding author: Department of Engineering and Technology, Manchester Metropolitan University, John Dalton Building, Chester Street, Manchester M1 5GD, UK. email: s.d.iwnicki@mmu.ac.uk

significance of flange contact. Rudd [**3**] discounts wheel squeal by differential slip or by flange contact alone, partly through experimental findings and with the hypothesis that the effect of the excitation forces is negligible as they are within the plane of the wheel.

Various theories, although much simplified, have evolved over the years to describe the creep force and creepage conditions during the excitation of a railway wheel in curves [**3–8**]. Generally, as creepage grows, the area of adhesion within the contact region decreases and the creep force increases until there is insufficient friction within the contact region to prevent sliding. The creep force then shows a falling characteristic with the adhesion coefficient reducing with increasing speed once the contact is sliding. It is noted here that besides the level of creepage, the creep force, and therefore, the friction force, is a function of normal load, material properties, and rolling velocity. It is thought that due to the falling curve, increased creep forces cannot be sustained and the creepage and creep force oscillate in a high-frequency limit cycle resulting in generation of squeal noise.

In the light of these theoretical findings, a model for predicting squeal noise has been developed [**9**] that includes a detailed representation of the dynamic behaviour of the wheel and rail and includes a contact model that allows for creepage in the saturated region including the effect of a falling adhesion coefficient. For the purpose of validating this squeal prediction model, a creep force/creepage relationship and a good set of acoustic/vibration measurements in a controlled environment were required and these data were obtained using a twin disc rig. These measurements included the lateral force due to varying amounts of lateral creep during squealing. Experimental results reported on the rolling contact force conditions during squeal include those by de Beer *et al.* [**6**], Monk-Steel *et al.* [**1**], and Brickle [**10**]. Only lateral creepage was considered in the current testing, as the effect of longitudinal creepage on squeal was found to be predictable in the light of the test results from previous tests [**1**]. Inclusion of longitudinal creep tends to reduce the lateral creep force and thereby change the slope of the friction curve. This leads to a lower incidence of squeal in the presence of longitudinal creep, and an increase in the threshold of lateral creepage necessary for squeal. Instrumentation on the rig was also specifically arranged to correspond to the input requirements of the squeal model.

This paper describes in detail the experimental work carried out during this project to validate the squeal prediction model together with a brief outline of the squeal model and preliminary comparison of the test results with the model and with relevant available theories.

2 THE TWIN DISC RIG

2.1 Test objectives

The rig, shown in Figs 1 and 2, was designed to investigate the squeal phenomenon due to unstable friction force with the following specific objectives:

(a) to simulate the wheel rail contact conditions as closely as possible in relation to curve squeal;
(b) to vary the lateral creepage at the contact point by changing the angle of attack of the wheel relative to the rail roller;
(c) to measure quasi-static changes in lateral force due to variation in lateral creepage;
(d) to measure the resonance frequency of the wheel roller in order to relate this to the spectrum of the measured squeal sound pressure;
(e) to investigate the effect of wheel speed;
(f) to vary the normal load at the contact point;
(g) to conform as closely as possible to assumptions made in theories, such as those of Kalker [**11**] that

Fig. 1 Overall view of the twin disc rig

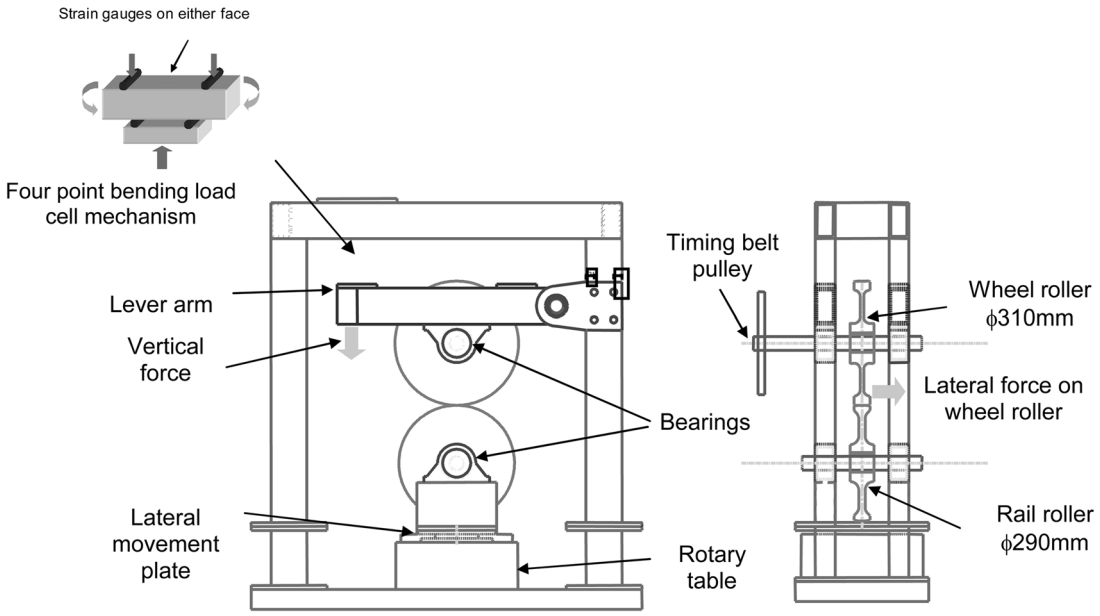

Fig. 2 Schematic of twin Disc rig

the bodies in contact have smooth surfaces, contact is elastic and that dry friction exists between them.

The input/output requirements of the rig are summarized in Table 1.

2.2 Rig description and test procedure

The layout of the rig is shown in Fig. 2. The rig consists of a steel wheel of 310 mm diameter, the wheel roller, which is driven at a constant speed, in contact with a similar wheel of slightly smaller diameter of 290 mm that is free to rotate in its bearings. Each roller was machined, and then ground to its final profile. Both wheels have a web and tyre arrangement. The wheel roller was scaled roughly to one-third of a UK Class 91 locomotive wheel, whereas the rail roller was designed to have a smooth transition to the tyre radius for ease of mounting damping material. The rail roller has a profiled radius of 100 mm machined around its periphery and a web thickness of 16 mm, whereas the wheel roller has a cylindrical profile and a web thickness of 9 mm. The 'point' contact between the rollers results in a contact patch size, assuming it to be elliptical and Hertzian with a normal load of 2.2 kN, of 1.19 mm by 0.97 mm. The resultant contact stress is the same as the full-size case. The addition of a web on the rail roller was essential for improving surface

Table 1 Input and output requirements

Inputs: vary and measure	Normal load	Up to 4 kN
	Contact patch lateral position on wheel	Adjust lateral offset of the wheel
	Lateral creepages	Adjust yaw angle
	Friction characteristics	Vary using lubricants or friction modifiers
	Vibration amplitude of wheel and rail rollers	Accelerometers
	Vibration response at three or more locations on wheel	To study whether forward or backward waves are excited
Outputs: measure	Noise spectra	Microphone close to wheel
	Vibration amplitude of wheel and rail rollers	Accelerometers
	Friction characteristics	Need to measure lateral quasi-static load as well as vertical load using strain gauges
Also to be measured	Wheel and 'rail' profiles	
	Modal and damping properties of wheel	Could also vary wheel damping
	Frequency response functions for 'rail'	Lateral and vertical. Need to ensure there is sufficient damping

strain sensitivity for measurement of the contact force, but its thickness is much larger than that of the wheel roller for a stiffer and more realistic representation of the rail. The rollers are made of EN24T steel with a nominal yield stress of about 650 MPa.

The wheel roller is mounted on a longer stub shaft supported in self aligning bearings mounted at the middle of a lever arm pivoted at one end onto a rigid frame. The shafts of the rollers are also made of EN24T steel and have a larger diameter at the hub. Slots were machined in each shaft for inserting the cables of a slip ring. Clearance fitting collars were inserted on either side of the shaft to react thrust loads. The shaft on top is mounted on the lever arm and the bottom one rigidly to the frame.

The lever arm provides the vertical force acting on the rollers through a jacking mechanism at the end of the arm. A rotary table on which the self-aligning bearings of the lower shaft are rigidly mounted allows a relative yaw angle between the rollers. This yaw angle is indicated by markings on the handle of the rotary table and also, more accurately, using a displacement transducer. Lateral adjustment is provided by sliding and locking the lateral positioning plate on which the bearings of the lower shaft sit.

The lever arm together with the wheel roller is normally clamped to the frame of the rig at the load cell position with a G-clamp to separate the rollers. Once the lateral position and the desired yaw angle is set, the lever arm is released onto the rail roller and contact pressure is applied through the hydraulic jack. Note that the ratio of the distance from the end of the lever arm to the distance of the axis of the rollers is 2 to 1, giving a vertical force acting on the rollers twice that of the applied hydraulic force.

Prior to each test series, the running surfaces of both rollers were first abraded with 600 and 1200 emery paper before being wiped dry with tissue and cleaned with degreaser. Having set-up the required contact condition, the inverter motor (10 kW, maximum speed of 3500 r/min) was started and a run-in period under load was allowed to ensure steady-state conditions before data acquisition was commenced in which a minimum ∼10 s was recorded per test. This duration was increased where transient conditions are also of interest, such as the period from non-squealing to squealing. The relatively short recording time was necessary to avoid the build-up of wear debris on the running surfaces, which appeared to be appreciable at large yaw angles and large normal loads under dry contact condition. By wiping the rollers between each reading, the amount of debris on the surface was kept relatively constant.

The rotation direction is fixed in one direction, i.e. the wheel roller rotates in a counter-clockwise direction driving the rail roller in the clockwise direction. The sign convention for the yaw angle defined here is positive for a clockwise turn on the handle of the rotary table. This results in a clockwise yaw angle of the rail roller. Therefore, considering the direction of rotation of the rollers, positive yaw will produce a lateral force at the contact patch coming out of the wheel roller as shown in Fig. 2 but a reaction force in the opposite direction on the rail roller.

Summarizing the main features of the twin disc rig, it fulfilled its main objectives as follows.

1. Lateral creep and hence lateral force was varied by changing the angle of yaw of the bottom roller relative to the top roller.
2. Lateral force was measured through a system of strain gauge bridges.
3. The ratio of the contact ellipse semi-axes was kept constant due to the constant radius profile of the rail roller and the cylindrical profile of the wheel roller.
4. Contact pressure was varied by changing the vertical load at the contact point.
5. The speed of the rollers was varied via the motor controller.
6. The contact surfaces were smooth (ground) and dry friction condition was maintained.

2.3 Instrumentation

The main instrumentation used was:

(a) low impedance voltage mode accelerometers;
(b) strain gauge bridges force measuring system set-up in a half-Wheatstone bridge configuration as shown in Fig. 3;

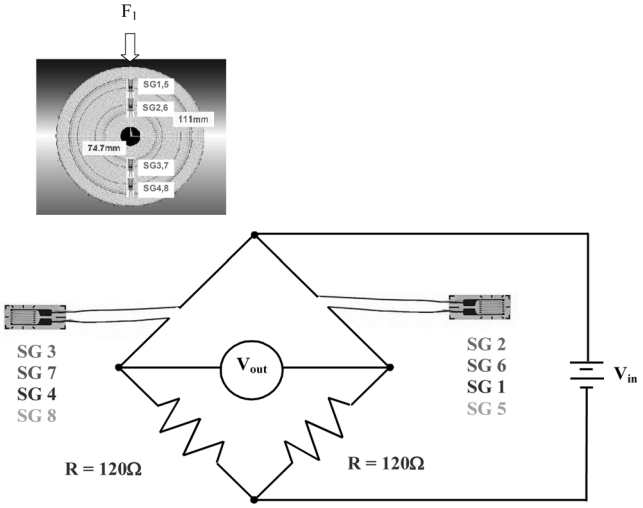

Fig. 3 Half-bridge configuration

(c) a displacement transducer for accurate measurement of the yaw angle;
(d) a precision sound level metre.

The force measuring system set-up was only intended for capturing the steady-state or quasi-static part and not the dynamic part of the contact force. Hence, the sampling frequency of 1000 Hz was deemed sufficient for a rolling speed of about 3.2 Hz. The radial positions of the strain bridges were determined as the optimum in terms of sensitivity and minimal cross-talk using a finite element (FE) model. Various bridge configurations were considered, but the bridge set-up shown in Fig. 3 was found to give the best sensitivity and a clean signal. The set-up meant that the force outputs are in the form of alternating peaks, which occur when the strain gauges are in line with the normal load. The two lateral force bridges give strain readings in opposite signs at large yaw angles to indicate compression and tension on opposite faces of the roller due to bending. By subtracting the two strain readings, strain due to the vertical force will be eliminated. The vertical bridges, on the other hand, show the same sign on both faces but when the average is taken, any bending strain will be eliminated. The adhesion coefficient is thus calculated as the ratio of the peak lateral force to the peak normal force.

All outputs were logged simultaneously by a data acquisition system. Two sampling rates were used, the higher of 10 kHz for the lateral vibration and sound pressure measurements and the rest at 1000 Hz. Commercial slip rings were used for connecting the cables of the strain gauges and accelerometers to the data logger.

2.4 Out-of-round measurements and calibration

Various preparatory tasks were carried out to ensure accurate and repeatable test results. These included initial measurements and calibration of the instrumentation and establishing a test procedure that included surface preparation for the rolling contact. These are described in more detail as follows.

With both rollers unloaded, the roundness of the rollers was measured three times successively at the middle of the running surface of the rollers using a displacement transducer. The maximum peak-to-peak out-of-roundness value of the rail roller was measured to be 0.03 mm and that for the wheel roller about 0.1 mm. These out-of-roundness were observed as a long-wavelength component in the vertical force measurement.

Calibration was carried out for all five strain bridges, including that of the load cell and the results are summarized as follows.

1. Load cell calibration – the sensitivity of the load cell was on average 65 $\mu\varepsilon$/kN.
2. Vertical load calibration – all strain outputs from the four half bridges increased linearly with the normal load at a variation of 12 mV/kN.
3. Lateral load calibration – the lateral strain bridges are about ten times more sensitive than the vertical strain bridge output at 120 mV/kN. It was also clear from the calibration results that the vertical bridge is relatively insensitive to any changes in the lateral load.

3 CREEPAGES AND CREEP FORCES

3.1 Creepages

The concept of creepage has been studied in the field of railway vehicle dynamics for many years and is well understood. However, the inclusion of the details of high levels of creepage, beyond the saturation regime of the contact forces has generally not formed part of the current vehicle dynamic simulation packages. As described earlier, it is this region where curve squeal is generated.

The definition of the coordinate system of the wheel and rail rollers is shown in Fig. 4. In the twin disc rig set-up, the rail roller is free to rotate and is driven by the wheel roller. When no slip occurs between rollers, the longitudinal creepage is virtually zero, i.e. $\gamma_1 = 0$. The lateral creepage is determined by

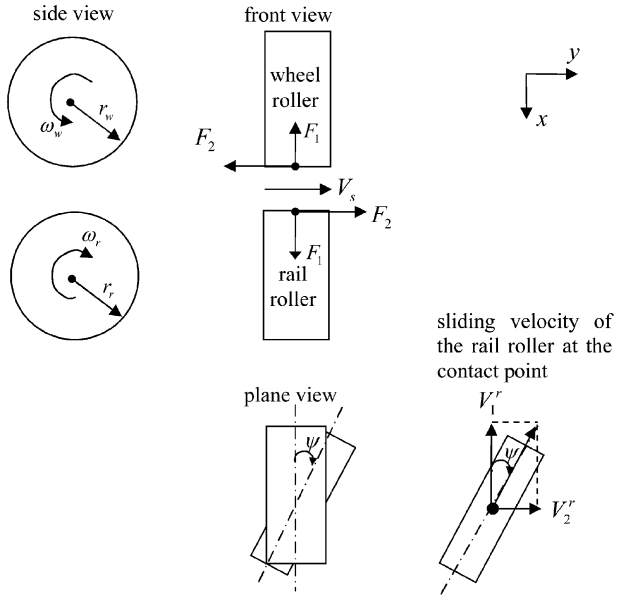

Fig. 4 Wheel and rail rollers coordinate system for twin disc rig and the squeal model

the yaw angle

$$\gamma_2 = \frac{V_2^{\mathrm{r}} - V_2^{\mathrm{w}}}{V} = \frac{r_{\mathrm{r}}\omega_{\mathrm{r}} \tan\psi - 0}{V} = \tan\psi \tag{1}$$

where, the lateral sliding velocity of the rail roller is $V_2^{\mathrm{r}} = r_{\mathrm{r}}\omega_{\mathrm{r}} \tan\psi$, lateral sliding velocity of the wheel roller is $V_2^{\mathrm{w}} = 0$, mean rolling speed of the wheel and rail rollers at the contact zone is $V = (r_{\mathrm{r}}\omega_{\mathrm{r}} + r_{\mathrm{w}}\omega_{\mathrm{w}})/2 = r_{\mathrm{r}}\omega_{\mathrm{r}}$, relative yaw angle between the rail roller and the wheel roller is ψ, angular velocity of the wheel/rail roller is $\omega_{\mathrm{r}}, \omega_{\mathrm{w}}$, and the radius of the wheel/rail roller is $r_{\mathrm{r}}, r_{\mathrm{w}}$.

As the contact plane is perpendicular to the vertical axis, assuming perfect vertical alignment of the rollers as shown in Fig. 4, the spin component can be assumed to be negligible.

3.2 Creep forces

In Kalker's linear theory, the lateral creep force is expressed as

$$F_2 = -f_{22}\gamma_2 - f_{23}\omega_3 \tag{2}$$

where, ω_3 is the spin creepage, and f_{22} is the Kalker's linear creep coefficient (N)

$$f_{22} = (ab)\, G\, C_{22} \tag{3}$$

where, a, b is the contact ellipse semi-axes (m), G the Shear modulus (N/m^2), and C_{22} the tabulated creep coefficient.

For the twin disc rig, $a = 1.19$ mm, $b = 0.97$ mm under a normal load of 2.2 kN, and $C_{22} = 1.553$. Ignoring the spin effect in equation (2) and substituting the lateral creepage from equation (1), the lateral creep force can be given as

$$F_2 = -f_{22} \tan\psi \tag{4}$$

Normally, the yaw angle is very small ($<2^\circ$) and equation (4) can be written as

$$F_2 \approx -f_{22}\psi \tag{5}$$

If the creep coefficient is constant, the lateral creep force is dependant only on the yaw angle and it is therefore easy to monitor the level of creepage through the yaw angle and establish the lateral creep force using a theoretical value of f_{22} for the linear section of the creep curve. Under a normal load of 2.2 kN, the twin disc rig gives f_{22} as 376 kN.

The adhesion coefficient is therefore defined as

$$\mu = -\frac{F_2}{F_1} \tag{6}$$

For large values of creep, the adhesion coefficient tends to the value of the friction coefficient and the above linear theory does not apply.

4 MODAL ANALYSIS AND TESTING

4.1 Finite element analysis

A modal analysis of the rollers was carried out using the FE package, ANSYS with the aim of establishing the resonant frequencies and vibration modes of the rollers for the effective positioning of accelerometers for measuring lateral vibration, and for establishing the frequency response function of the rollers under forced vibration in order to ensure realistic and correct assessment of the measured data.

Each roller model was constructed using >10 000 three-dimensional brick elements (solid45), each of which has eight nodes. The surface of the hub was restrained in all directions, and the modal damping ratio was set as 0.0001 to ensure the response at the resonances did not tend to infinity. The modal analysis covered frequencies of up to 15 kHz.

4.2 Modal testing

The aim of this test was to obtain the modal properties of the rollers over a frequency range up to 5 kHz, as the predominant squeal frequency is thought to be in the 2 kHz range. Both rollers were set-up on their respective shafts. Each roller was tapped three times in the lateral direction as close to the contact point as possible with an instrumented hammer, and the resultant lateral excitation of the roller was recorded by an accelerometer at a sampling rate of 20 kHz for an effective frequency band of 10–10 kHz.

4.3 Results and discussion

The natural frequencies of the two rollers obtained from the FE modal analysis are listed in Table 2

Table 2 Predominant natural frequencies of the wheel and rail rollers

	Wheel roller		Rail roller	
(n, m)	Predicted	Measured	Predicted	Measured
(2,0)	1089	1094	1512	1460
(3,0)	2851	2874	2969	3143
(4,0)	5223	5283	5558	5533
(5,0)	8032	7983	8415	8500

n: nodal diameters on the roller plane; m: nodal circles on the roller plane.

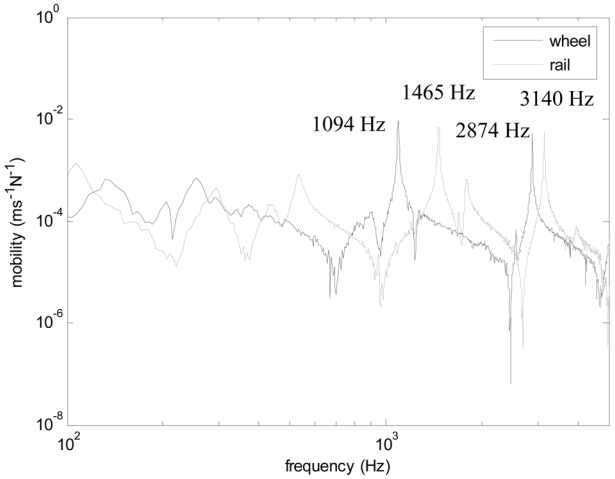

Fig. 5 Lateral measured mobilities of the wheel and rail rollers: ——— wheel, ----- - rail

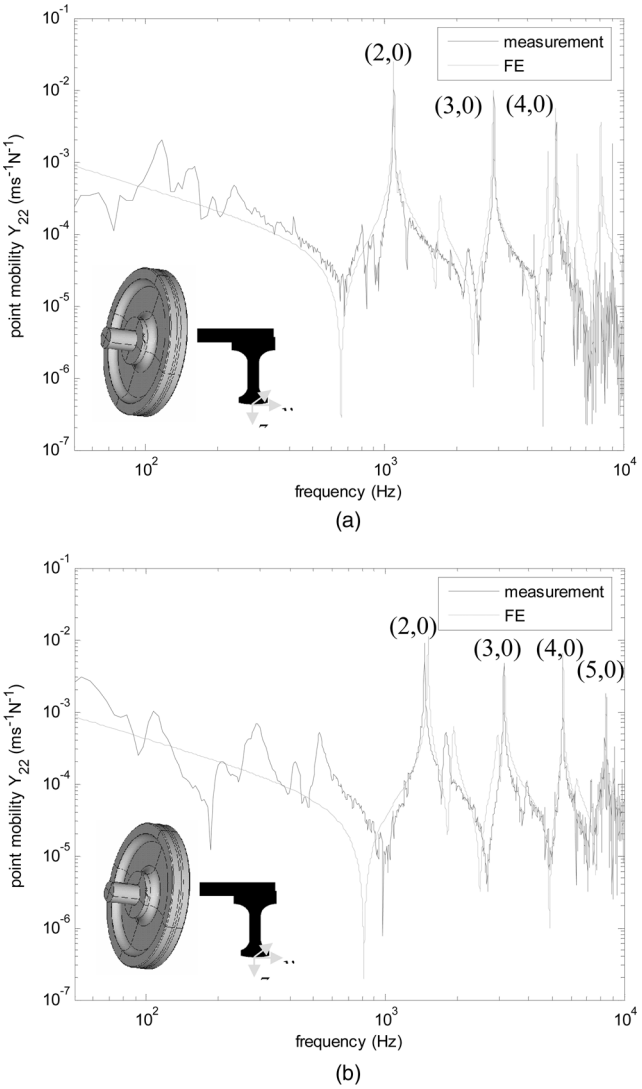

Fig. 6 Lateral mobility: ——— measured, ----- - FE analysis (a) wheel roller and (b) rail roller

together with experimental results, with no damping and with damping material fixed to the rail roller. Notably, the FE model exhibited the typical feature of an axisymmetric structure with modes existing in pairs, i.e. two modes with identical natural frequencies and mode shapes which differ only in the angular orientation of the nodal lines [**12**].

During the design stage, the rail roller was redesigned several times to ensure that its resonant frequencies did not coincide with those of the wheel roller at or around the squeal frequencies to avoid interference of the squeal frequencies of the two rollers. This is clearly seen by comparing the measured lateral mobilities of the wheel and the damped rail roller, as shown in Fig. 5, the two dominant natural frequencies of the wheel, 1094 and 2874 Hz, are lower than those of the rail roller, 1465 and 3140 Hz, respectively. This appreciable difference enables the squeal source to be easily distinguished from the spectral analysis of the radiated sound.

The lateral mobility curves are compared with the results from the FE analysis shown in Fig. 6. At first, the FE models were built without an attached axle, but due to the poor mobility prediction for the rail roller, a truncated axle was included in both models to increase flexibility at the hub. This resulted in better correlation as shown in Fig. 6. From animations in the FE analysis, it is noted that at the lower frequency range (<1000 Hz) the predicted first two modes correspond to the dishing of the rollers and the first wheel axial mode. In the frequency range of 1000–5000 Hz, the predicted mobility of both the wheel and rail roller agrees well with the measurements.

5 CREEP FORCE AND DYNAMIC RESPONSE MEASUREMENTS

To ensure that the contact conditions between the rollers conform as closely as possible to the assumptions made in the rolling contact theories of 'dry' and smooth running conditions, fairly high contact pressure and relatively low running speed were used to minimize roughness effects. In the creep force measurement, three test series were carried out, namely, investigating the effect of speed, investigating creepage variation with and without damping of the rail roller.

5.1 Speed test

To find the effect of varying rolling speed, the adhesion coefficient was checked by running the

rollers continuously and increasing the motor speed in steps. The test settings for this test case were as follows:

(a) normal load of ∼1.8 kN;
(b) a yaw angle of 0.3°;
(c) variation of the motor speed from 1.6 to 5.5 rev/s giving a nominal wheel roller speed of 19–65 rad/s (2.9–10.1 m/s);
(d) no lateral displacement offset;
(e) sampling frequency of 10 kHz for accelerations and the sound pressure level and 500 Hz for the force and displacement measurements.

The readings taken at each yaw angle were as follows:

(a) lateral acceleration at the rim of the wheel roller;
(b) lateral acceleration at the rim of the rail roller;
(c) strain bridge reading for the vertical load on the web face of the rail roller under compression;
(d) strain bridge reading for the vertical load on the web face of the rail roller under tension;
(e) strain bridge reading for the lateral load on the web face of the rail roller under compression;
(f) strain bridge reading for the lateral load on the web face of the rail roller under tension;
(g) yaw angle;
(h) normal load applied at the load cell;
(i) sound pressure level.

Error in the measured adhesion coefficient is a combination of the uncertainties in the measured normal and lateral forces, i.e. $\delta\mu = \sqrt{(\delta F_2/F_2)^2 + (\delta F_1/F_1)^2}$, where the prefix δ denotes uncertainty. Assuming an uncertainty of 10 per cent for both forces, then the uncertainty in μ is ±14 per cent as shown by the error bars in Fig. 7, where the adhesion coefficient from the speed test is plotted against the rolling velocity. It is apparent that the adhesion coefficients remain fairly constant between the rolling speed of 1.6 and 5.5 m/s and fall within the error estimate. Nonetheless, it is recognized that a more thorough series of tests investigating the magnitude of third-body abrasive behaviour on wear for steady-state conditions, including roughness measurements and scanning electron microscope observations, is required to further understand the changes in the adhesion coefficient at the contact patch during squeal.

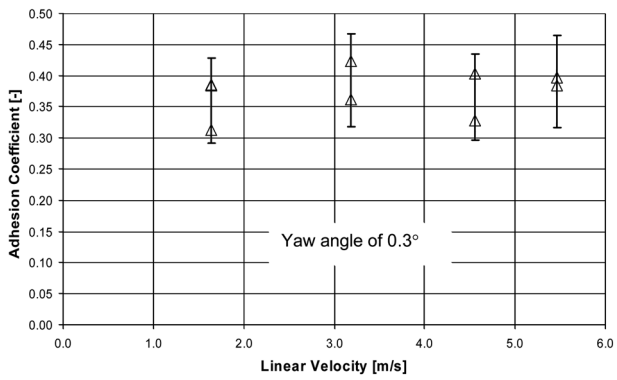

Fig. 7 Effect of varying rolling speed on adhesion coefficient

5.2 Creepage variation tests

The test settings were the same as before but with a normal load of ∼2.2 kN, a constant motor speed of 1.7 rev/s, resulting in a nominal wheel roller speed of 20 rad/s and a nominal rail roller speed of 21.4 rad/s (3.1 m/s), and the yaw angle was varied from negative to large positive angles.

Two test cases were carried out, the first with no damping material and the second with damping material added to the rail roller (as described above). In each case the yaw angle of the rail roller was varied, simultaneous measurements of contact forces, lateral vibration of the rollers at the tyre and the sound pressure level were made. Figures 8 to 10 show typical results obtained for varying the lateral creepage, in this case where the yaw angle was 0.85°, the rail roller was damped and squeal was heard. Figure 8 shows the power spectral density of the lateral acceleration of the rollers and the sound pressure level, with indication of the dominant frequencies (1490 and 1090 Hz) present in the event of squeal; Fig. 9 shows the change in adhesion coefficient through the duration of the test.

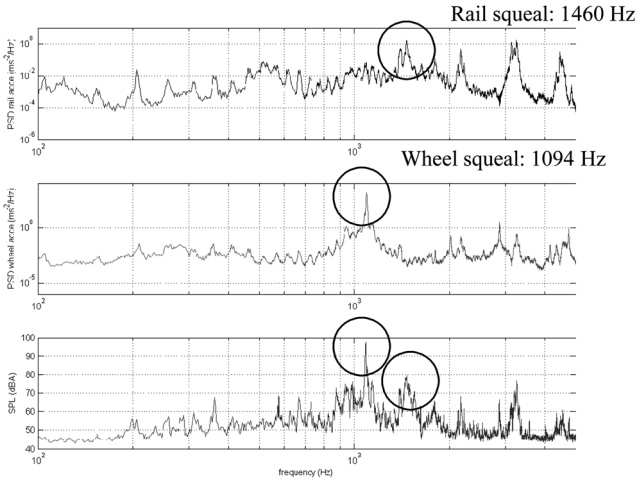

Fig. 8 Power spectral density of the lateral acceleration of the rollers and the sound pressure level

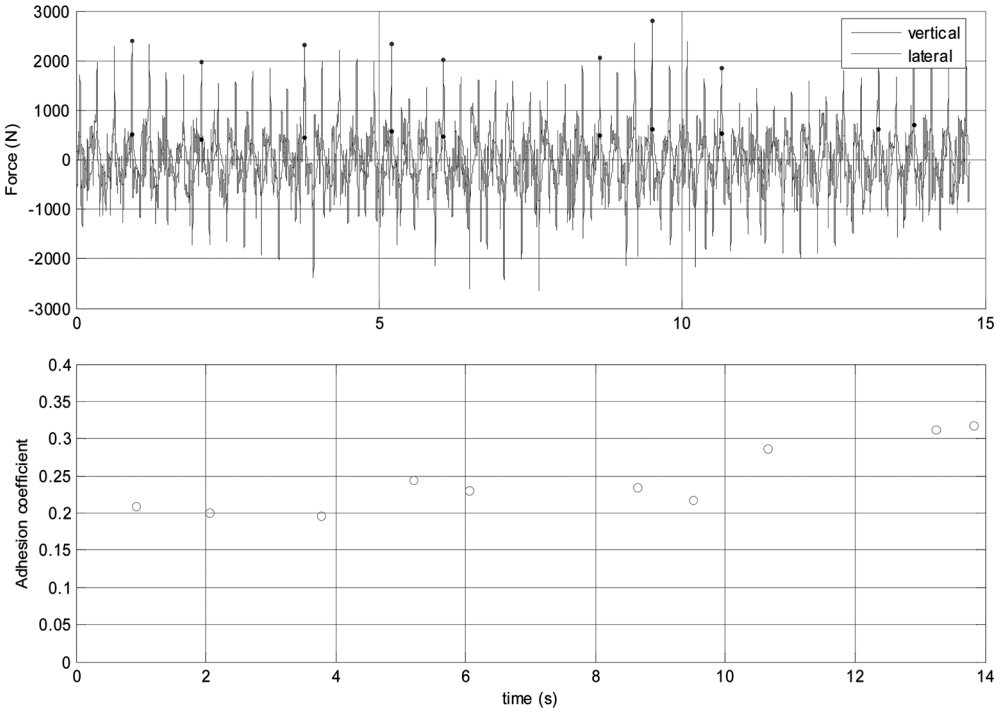

Fig. 9 Variation of creep force and adhesion coefficient in test with a yaw angle of 0.85° and a normal load of 2.2 kN

5.3 Validity, accuracy, and repeatability of results

The main objective of the experimental investigation was to provide controlled test data for the lateral force and therefore adhesion coefficient due to varying amounts of lateral creep in rolling contact with and without squeal using a twin disc rig. Despite the absence of actual rail and wheel transverse profiles on both rollers, conditions existing on the rig were similar in many respects to the actual condition between a railway wheel and the rail and squeal of comparable frequency and frequency range was generated. Most importantly, however, the contact conditions on the twin disc rig conformed as closely as possible to assumptions made in rolling contact theories in that 'dry' and smooth running conditions were maintained under fairly high contact pressure and relatively low running speed to minimize roughness effects. This is necessary for comparison with theories and with the squeal prediction model developed [**9**].

In general, the system was stable with no undesirable oscillation up to the tested yaw angle of ±2°. The main test measurements were the contact forces and the associated lateral vibration of the rollers. The signals from the force gauges show distinct maximum and minimum values for calculating the adhesion coefficients with the vertical force measured by the strain gauges within 10 per cent of that measured by the load cell. The creep characteristics were found to be repeatable with the linear slope of the data in the creep force versus creepage curve agreeing well with theory and the yaw angles at which squeal noise occurred were repeatable and consistent. The power spectral density of the signals from the accelerometers and sound pressure metre also agreed well with each other as shown in Fig. 8.

At moderately large yaw angles, a quiet ringing was heard while at large angles of yaw, the wheel roller was seen to vibrate in the lateral direction while generating a high pitch squealing noise. The cause of this could be a reduction in the effective coefficient of friction at the contact point. Wear debris was also found after each test evident from the black debris from cleaning the running surfaces. For these reasons, tests were generally not allowed to run for a long period and yaw angles were restricted to within ±2° to ensure repeatable results.

5.4 Comparison with theory

In general, the measured adhesion coefficient remains relatively constant for the first few seconds of each run (within ±14 per cent) until after 10 s when it appears to increase. This is seen in Fig. 9 for the condition of 0.85° yaw angle and a normal load of 2.2 kN. The adhesion coefficient appears to increase gradually at first and then more apparently after

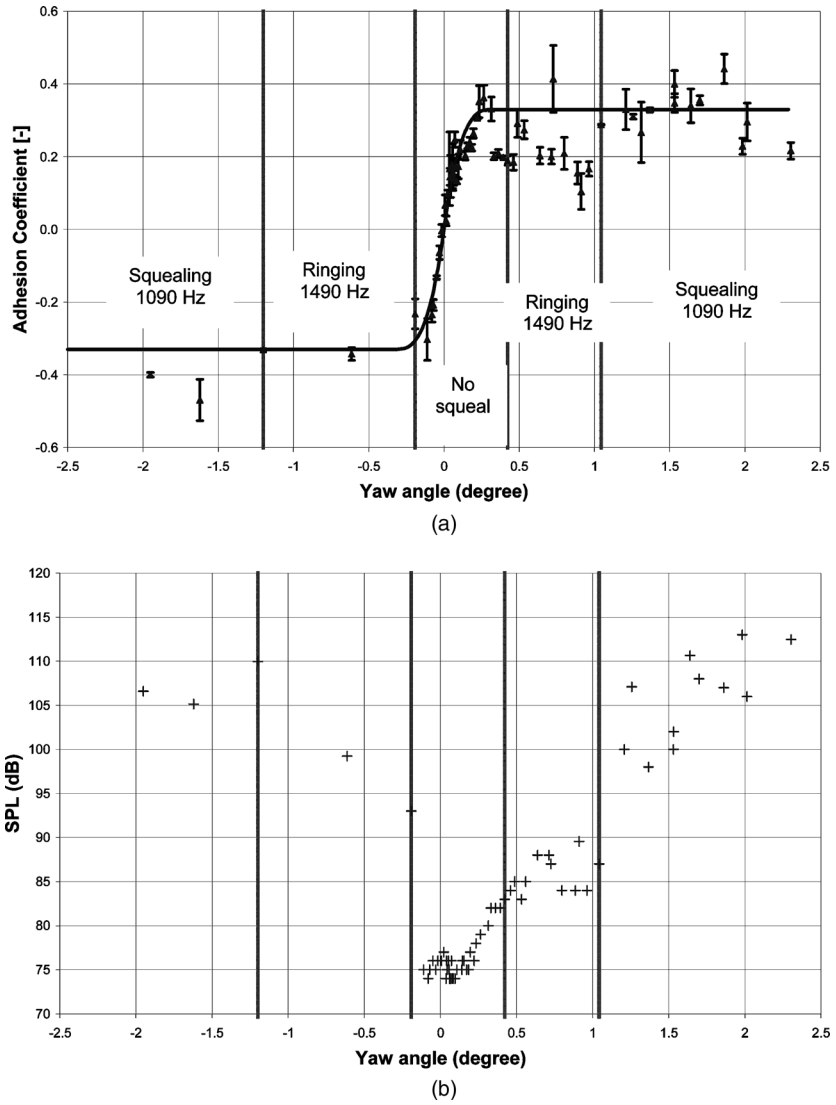

Fig. 10 Test case with no damping on rail (a) adhesion coefficient versus yaw angle, Δ: experimental - -: Shen *et al.* [**13**] and (b) sound pressure level of the dominant frequency versus yaw angle

10 s from 0.2 to 0.32. When plotting the adhesion coefficient for each yaw angle in the force versus creepage curve, the average of these points was taken, in this case, 0.24. It is clear from the error bars in Figs 10 and 11 that the adhesion coefficient can fluctuate between ± 0.1 from the average value for each test, particularly during squealing. It is therefore evident that more detailed examination into the influence of third-body behaviour under steady-state condition is required to validate the use of the average adhesion coefficient.

It was found in the test case with no damping on the rail roller that quiet ringing started at about 0.42°, whereas full squeal started at about 1°. After damping material was added, ringing occurred earlier at about 0.3° and squeal at 0.45°. On the basis of the analysis of the power spectral density of the lateral acceleration of the rollers and the sound pressure level, an example of which is shown in Fig. 8, the sound radiation can be classified as follows:

(a) wheel and rail rollers are stable, no squealing: <80 dB(A);
(b) wheel and rail roller vibration increased, rail response is larger than wheel, the rail mode at 1490 Hz is predominant in the sound radiation, ringing: $80 \sim 90$ dB(A);
(c) wheel roller is unstable and response is much larger than that of the rail roller, the wheel mode

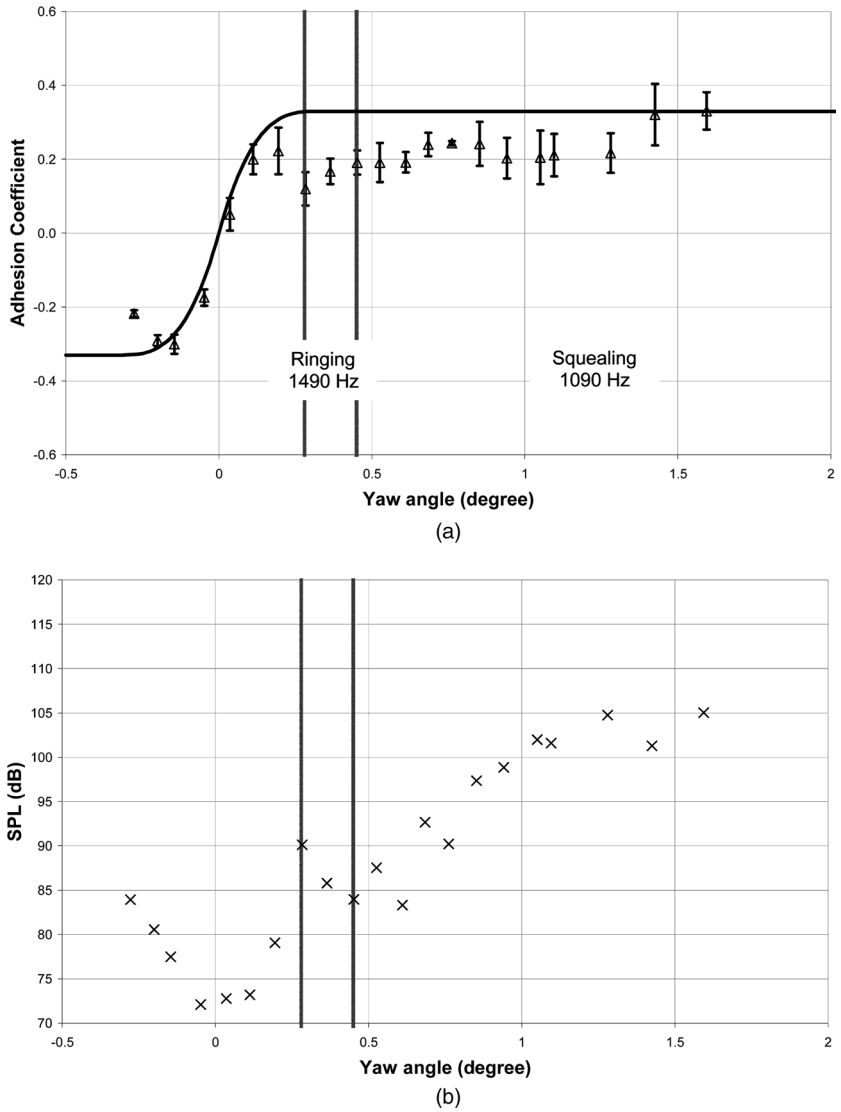

Fig. 11 Test case with damping on rail (a) adhesion coefficient versus yaw angle, Δ: experimental - -: Shen *et al.* [**13**] and (b) sound pressure level of the dominant frequency versus yaw angle

at 1090 Hz is predominant in the sound radiation, squealing: 90 $\sim$ 110 dB(A).

It is noted that for the The Netherlands Organisation for Applied Scientific Research (TNO) rig [**1**] which was also one-third scale, the start of squeal noise under pure lateral creepage occurred at 0.3° at a base frequency of 1150 Hz for a normal load of 1 kN and speed of 1.2 m/s.

The creep force and creepage relationships for the two test cases are shown in Figs 10 and 11, respectively, with the theoretical prediction by Shen *et al.* [**13**] for comparison. Having adjusted for the zero yaw datum, it is clear that the adhesion coefficient curve appears symmetrical about the yaw datum. The curve increases linearly up to about 0.1° where it levels off to a peak at about 0.2° before falling rapidly and then increasing again. For yaw angles >2°, the curve decreases again. It is noted that during the rapid fall in the adhesion coefficient, a ringing sound was heard and when the wheel was squealing the adhesion coefficient increases again. The comparison with the prediction is good in the linear regime. From the error bars, it is clear that the fluctuation of the adhesion coefficient for a tested yaw angle appears to be generally more pronounced during squeal.

The measured adhesion coefficient data is compared with the Fingberg formula [**4**] where its coefficient, κ was adjusted to 0.05, for the best fit to the experimental data and shown in Fig. 12. The agreement is good for the range of yaw angle tested for the two test cases but deviates for the case with damping material when the yaw angle exceeds 1.5°.

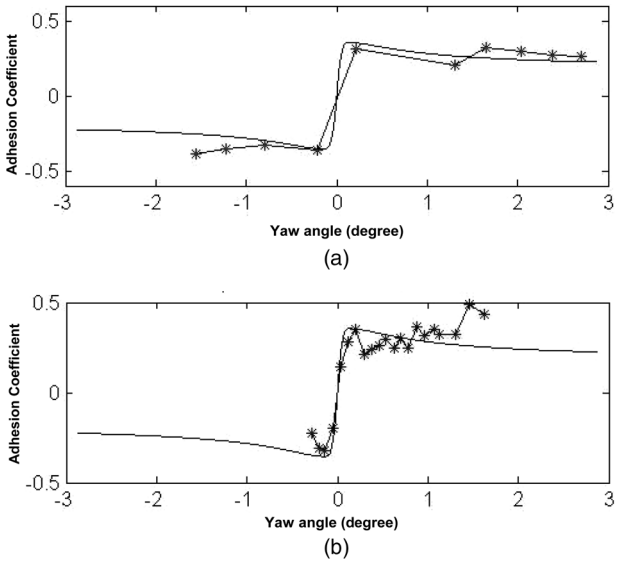

Fig. 12 Comparison of adhesion coefficient: ——from Fingberg's formula [**4**], *measured adhesion coefficient (a) no damping on rail and (b) with damping on rail

6 CURVE SQUEAL MODEL

6.1 Introduction

A brief outline of the squeal prediction model in the frequency domain that is simplified and used for comparison with the experimental data is now given. The squeal prediction model is based on the work of de Beer *et al.* [**9**], which includes a detailed wheel/rail contact model and mainly considers the instability of wheel/rail system because of the lateral creep force. However, in this simplified squeal prediction model, the vertical force is assumed to be constant by ignoring the vertical fluctuating force because of the lateral sliding velocity. This simplification focuses the squeal prediction work only on the effect of lateral creep force.

The model is derived on the basis that the forces and velocities can be expressed as a quasi-static part and a fluctuating part. For the wheel and rail rollers shown in Fig. 4, the lateral creep force acting on the rail $F_2 = F_{20} + f_2(t)$, the lateral sliding velocity $V_s = V_2^r - V_2^w = V_{s0} + v_s(t)$ and the lateral creepage $\gamma_2 = \gamma_{20} + v_s(t)/V$ consist of a steady-state part and a time-variant part. The vertical force (normal load) is assumed to be constant $F_1 = N_0$. Thus, the lateral creep force can be written as

$$F_{20} + f_2(t) = -N_0\mu\left(\gamma_{20} + \frac{v_s(t)}{V}\right) \tag{7}$$

where the quasi-static parts in equation (7) have the following relationship

$$F_{20} = -N_0\mu(\gamma_{20}) \tag{8}$$

Since, for the stability analysis, the amplitude of the time-variant sliding velocity v_s can be considered to be very small, the non-linear adhesion coefficient $\mu(\gamma)$ in equation (7) can be linearized around γ_{20}. Thus, after eliminating the quasi-static parts, the fluctuating friction force in equation (7) can be expressed in the frequency domain as

$$F_2(\omega) = -\frac{N_0}{V}\frac{\partial\mu(\gamma_{20})}{\partial\gamma}V_s(\omega) \tag{9}$$

The sliding velocity is the combination of wheel and rail fluctuating velocities, and can be expressed as

$$V_s(\omega) = Y_y F_2(\omega) \tag{10}$$

where Y_y is the combination of lateral mobilities of wheel and rail rollers

$$Y_y = Y_y^w + Y_y^r \tag{11}$$

The inter-relationship between sliding velocity and creep force in equations (9) and (10) can be described by a loop, as shown in Fig. 13, which starts from a small and transient disturbance F_2' and develops the sliding velocity V_s and consequently creep force F_2 through the positive feedback.

The open loop transfer function is given by

$$H(\omega) = -\frac{N_0}{V}\frac{\partial\mu(\gamma_{20})}{\partial\gamma}Y_y \tag{12}$$

The instability of the positive feedback system can be determined by the Nyquist criterion, which states that the closed loop system is unstable (the disc squeals) for frequencies where the real parts of open loop gain $H(\omega)$ in equation (12) are greater than unity and the phases are zero (for those positive feedback cases).

6.2 Correlation with squeal model

Two cases with different creepages, $\gamma_{20} = 0.002$ and $\gamma_{20} = 0.023$, are provided to show the effectiveness of the squeal prediction. The normal load $N_0 =$

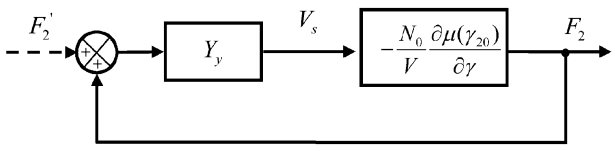

Fig. 13 Feedback loop between sliding velocity and the friction force

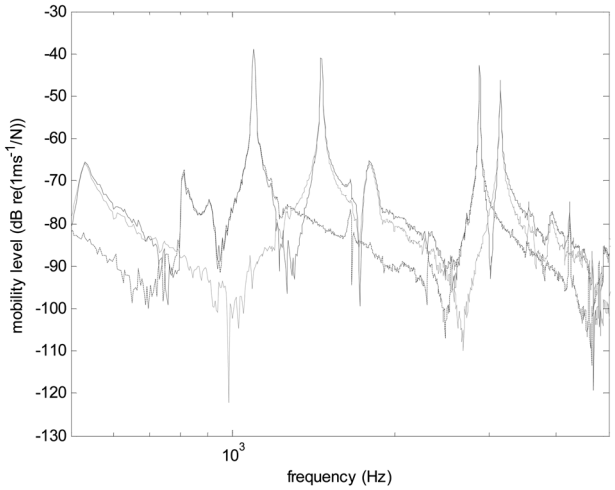

Fig. 14 Measured mobility curves of wheel roller — —, rail roller, - - - - and the combination of wheel and rail ——

1760 N, the rotating speed at the contact position $V = 3.2$ m/s, the measured lateral mobilities of wheel and rail rollers shown in Fig. 14 and the adhesion coefficient shown in Fig. 12 are adopted to calculate the open loop gain in equation (12). The frequency range considered here is in the region 500–5000 Hz.

For the case of small creepage $\gamma_{20} = 0.002$, the slope of the adhesion coefficient at this quasi-static creepage is positive: $\partial\mu/\partial\gamma = 85.3$, which means the creep force has damping effects on the system and suppress the vibration of wheel and rail rollers. In Fig. 15(a), the real parts of the open-loop gain with zero phase at these frequencies (normally they are the modes of

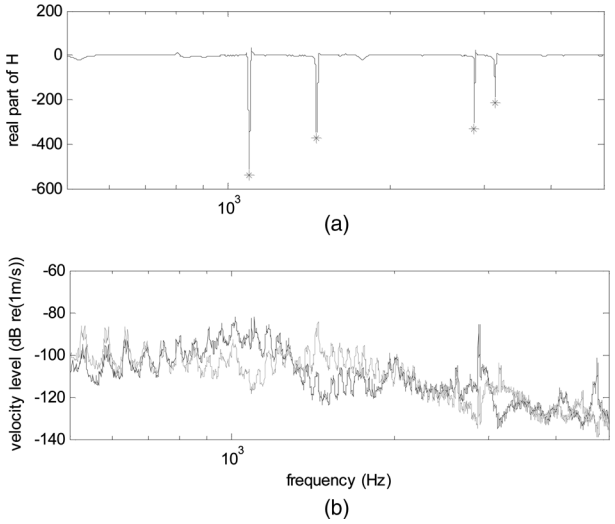

Fig. 15 Comparison of squeal prediction and roller vibration for creepage 0.002, (a) squeal prediction results, *the real part of the open loop with zero phase angle; (b) lateral velocities of the wheel and rail rollers, —— wheel, ----- rail

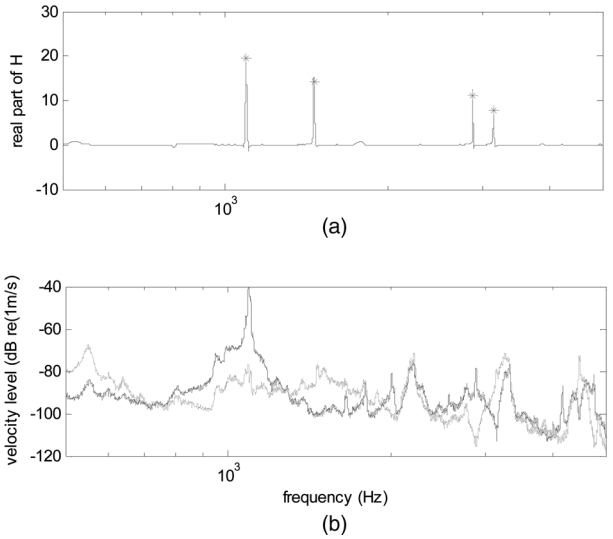

Fig. 16 Comparison of squeal prediction and roller vibration for creepage 0.023, (a) squeal prediction results, *the real part of the open loop with zero phase angle; (b) lateral velocities of the wheel and rail rollers, —— wheel, ----- rail

the wheel and rail rollers) are all negative, indicating that the responses at these frequencies are heavily damped, as shown in Fig. 15(b). The model therefore predicts that no squeal is generated at this small quasi-static creepage.

However, if the creepage is very large, for example, in the case with $\gamma_{20} = 0.023$, the slope of the adhesion coefficient is negative $\partial\mu/\partial\gamma = -3.3$, which means the creep force contributes negative damping effects to the system and subsequently destabilizes selected modes. In Fig. 16(a), it is clear from the squeal model that the system is unstable at four frequencies, corresponding to the most flexible modes of the wheel and rail rollers in this frequency range. The dominant frequency of these unstable frequencies is about 1092 Hz, one of the dominant modes of the wheel roller. The harmonics of this dominant frequency are found at about 2200, 3300, and 4400 Hz in the wheel response, as shown in Fig. 16(b).

The main conclusion drawn from the squeal model comparison is that the squeal phenomenon is strongly related to the properties of the adhesion coefficient. A small creepage with positive slope on the force/friction curve maintains the stability of the system and suppresses squeal. On the other hand, large creepage with negative slope on the friction curve leads to instabilities of the system at a specific mode that was well predicted by the squeal prediction model. Consequently, squeal is emanated at this dominant unstable mode together with its high-frequency harmonics. It should be pointed out that the squeal prediction model is based on the linearization of the adhesion coefficient curve at the

quasi-static creepage point. Thus, the model is only effective for cases where the quasi-static creepage is located near or about the zone where the relationship between the creepage and the adhesion coefficient is approximately linear.

7 CONCLUSIONS

A twin disc rig has been successfully developed for the purpose of investigating the squeal phenomenon due to unstable lateral creepage. Measurements have been taken of the modal response of the two rollers and the creepage-dependent adhesion coefficient in rolling contact by varying the lateral creepage through varying the yaw angle between the rollers. The relationships between the non-linear adhesion coefficient, the modal properties of the rollers with regard to squealing have also been established.

In the modal analysis, the predicted wheel and roller mobilities agreed well with the measurements in the frequency range of 1000–10 000 Hz. These were then input into the squeal prediction model together with the contact force condition for validation purposes.

In general, the creepage variation test results were repeatable and consistent and comparison with theory and the squeal prediction model was reasonable. It was found in the test case with no damping on the rail roller that quiet ringing started at about 0.42°, whereas full squeal started at about 1°. After damping material was added, ringing occurred earlier at about 0.3° as with squeal at 0.45°. The results showed that the sound pressure level can be classified into three types, namely, no squealing, rail roller squealing, and wheel roller squealing.

The main conclusion drawn from the squeal prediction model comparison was that the squeal phenomenon was strongly related to the properties of the adhesion coefficient. A small creepage with positive slope on the force/friction curve maintained the stability of the system and suppressed squeal. On the other hand, large creepage with negative slope on the friction curve leads to instabilities of the system at a specific mode that was well predicted by the squeal model. A time-domain squeal model is currently under development that would eventually be used to predict squeal amplitude as well as the unstable modes. The model will be validated using the twin disc rig.

ACKNOWLEDGEMENTS

The authors are grateful to the Engineering and Physical Sciences Research Council for supporting this project through Rail Research UK.

REFERENCES

1 **Monk-Steel, A. D., Thompson, D. J., de Beer, F. G.,** and **Janssens, M. H. A.** An investigation into the influence of longitudinal creepage on railway squeal noise due to lateral creepage. *J. Sound Vib.*, 2006, **293**, 766–776.

2 **Remington, P. J.** Wheel/rail squeal and impact noise: what do we know? What don't we know? Where do we go from here? *J. Sound Vib.*, 1987, **116**, 339–353.

3 **Rudd, M. J.** Wheel/rail noise-part II: wheel squeal. *J. Sound Vib.*, 1976, **46**(3), 381–394.

4 **Fingberg, U.** A model of wheel-rail squealing noise. *J. Sound Vib.*, 1990, **143**, 365–377.

5 **Schneider, E., Popp, K.,** and **Irretier, H.** Noise generation in railway wheels due to rail-wheel contact forces. *J. Sound Vib.*, 1988, **120**(2), 227–244.

6 **de Beer, F. G., Janssens, M. H. A., Kooijman, P. P.,** and **van Vliet, W. J.** Curve squeal of railbound vehicles (part 1): frequency domain calculation model. Proceedings of Internoise, Nice, France, 2000, vol. 3, pp. 1560–1563.

7 **Kooijman, P. P., van Vliet, W. J., Janssens, M. H. A.,** and **de Beer, F. G.** Curve squeal of railbound vehicles (part 2): set-up for measurement of creepage dependent friction coefficient. Proceedings of Internoise, Nice, France, 2000, vol. 3, pp. 1564–1567.

8 **Janssens, M. H. A., van Vliet, W. J., Kooijman, P. P.,** and **de Beer, F. G.** Curve squeal of railbound vehicles (part 3): measurement method and results. Proceedings of Internoise, Nice, France, 2000, vol. 3, pp. 1568–1571.

9 **de Beer, F. G., Janssens, M. H. A.,** and **Kooijman, P. P.** Squeal noise of rail-bound vehicles influenced by lateral contact position. *J. Sound Vib.*, 2003, **267**, 497–507.

10 **Brickle, B. V.** *The steady state forces and moments on a railway wheelset including flange contact conditions*. Thesis, Department of Transport Technology, Loughborough University of Technology, 1973.

11 **Kalker, J. J.** *Three dimensional bodies in rolling contact*, 1990 (Kluwer Academic Publishers, Dordrecht).

12 **Ewins, D. J.** Modal testing: theory, practice and application, 2nd edition, 2000 (Research Studies Press Ltd, Baldock, England).

13 **Shen, Z. Y., Hedrick, J. K.,** and **Elkins, J. A.** A comparison of alternative creep force models for rail vehicle dynamics analysis. Proceedings of the 8th IAVSD Symposium, Cambridge, Massachusetts, 1983, pp. 591–605 (Swets & Zeitlinger, Lisse).

APPENDIX

Notation

a, b	contact ellipse semi-axes (m)
C_{22}	tabulated creep coefficient
$f_2(t)$	time variant part of F_2 (N)
f_{22}, f_{23}	Kalker's linear creep coefficient, (N)
F_1, N_0	normal force (N)
F_2	lateral creep force (N)
F_{20}	quasi-static part of F_2 (N)
G	Shear modulus (N/m^2)
$H(\omega)$	open loop gain

r_r radius of the rail roller (m)
r_w radius of the wheel roller (m)
$v_s(t)$ time variant part of V_s(m/s)
V mean rolling speed of the wheel and rail rollers at the contact zone (m/s)
V_s lateral sliding velocity (m/s)
V_{s0} quasi-static part of V_s(m/s)
V_2^r lateral sliding velocity of the rail roller (m/s)
V_2^w lateral sliding velocity of the wheel roller (m/s)
Y_y^w lateral mobility of the wheel roller (m/s/N)
Y_y^r lateral mobility of the rail roller (m/s/N)
Y_y combination of the lateral mobilities of wheel and rail rollers (m/s/N)

γ_1 longitudinal creepage
γ_2 lateral creepage
γ_{20} steady-state part of γ_2
μ adhesion coefficient
ψ the relative yaw angle between the rail roller and the wheel roller (°/rad)
ω_r angular velocity of the rail roller (rad/s)
ω_w angular velocity of the wheel roller (rad/s)
ω_3 spin creepage